Nanocomposite Foams from High-Performance Thermoplastics

L. Sorrentino,[1,2] M. Aurilia,[2] L. Cafiero,[1] S. Iannace[1,2]

[1]*Institute for Composite and Biomedical Materials–National Research Council (CNR); Piazzale Tecchio 80, 80125 Naples, Italy*
[2]*Technological District on Polymeric and Composite Materials Engineering and Structures (IMAST), Piazzale Enrico Fermi 1, località Porto del Granatello, 80055 Portici (Naples)*

Received 28 April 2011; accepted 28 April 2011
DOI 10.1002/app.34784
Published online 11 August 2011 in Wiley Online Library (wileyonlinelibrary.com).

ABSTRACT: The foaming processes of nanocomposites based on high-performance thermoplastic polymers, namely, poly(ether sulfone) (PES; amorphous) and poly (ethylene-2,6-naphthalate) (PEN; semicrystalline), reinforced by two nanofiller types (expanded graphite and SiO_2 nanopowder), were investigated. Matrices were prepared by melt blending through extrusion, and a good dispersion of particles was achieved, as confirmed by microscopic and X-ray diffraction analyses. A solid-state foaming technique was used to prepare the foams; the samples were solubilized with carbon dioxide and quickly heated in an oil bath to the selected foaming temperature. The effects of both the type and concentration of the filler and the polymer type (amorphous and semicrystalline) on the cellular morphology were analyzed. Foams prepared from PES-based nanocomposites showed microcellular morphologies and higher numbers of nucleated cells (up to 10^{11} cells/cm^3), but low expansion ratios were achieved compared to PEN-based foams. Both SiO_2 and graphite nanoparticles acted as cell nucleating agents in the PES nanocomposites, but the latter gave better results, increasing the cell number by two orders of magnitude with respect to the neat polymer. This behavior was attributed to either the heterogeneous nucleation of cells or the improved barrier to gas diffusion of the graphite nanoplatelets with respect to SiO_2 nanoparticles. The PEN nanocomposite foams exhibited low foam densities, but fewer cells were nucleated with respect to the PES nanocomposites. The increase in the crystallization rate related to the presence of fillers, in particular when graphite was used, affected the expansion ratio at high foaming temperatures. © 2011 Wiley Periodicals, Inc. J Appl Polym Sci 122: 3701–3711, 2011

Key words: foams; high performance polymers; morphology

INTRODUCTION

The growing need to reduce weights in high-performance applications, such as in the automotive, transport, and aeronautic industries, has led to the wider use of foams in lightweight structures, such as sandwich structures, and in applications where low thermal, acoustic, and electric conductivities are required. Conventionally, polymeric foams are employed in many applications, such as packaging, thermal, and acoustic insulation, and in the absorption of impact energy. The service temperatures of these conventional applications are not much different from room temperature,[1] but a stringent requirement in high-performance applications is the resistance of foams to high temperatures.[2–4]

To maximize the mechanical properties of foams after the linear elastic region, a microcellular [with a cell density (N_0; the number of cells nucleated per unit volume of the original unfoamed polymer) of at least 10^9 cells/cm^3 and a diameter of less than 10 μm[5–7]], closed-cell structure should be produced. Today, very few high-performance microcellular foams are available on the market, probably because of the difficulties in manufacturing. They are often based on thermosetting polymers and are usually produced through complex and long processes, such as foaming from low-molecular-weight precursors[8] or stabilization of the cellular structure by polymer crosslinking.[9]

Because of their several advantages over thermosetting polymers (higher impact strength, recyclability, weldability, absence of volatile organic compounds, reduced processing time, and lower manpower), thermoplastics are preferred, but a complete understanding of the foamability conditions of high-performance thermoplastic matrices is still ongoing.[10]

The use of inorganic fillers is a common practice in the plastics industry for improving cell nucleation and some physical properties, such as the heat distortion temperature, hardness, toughness, and stiffness. The effects of filler addition on the mechanical and other properties depend strongly on the filler's

Correspondence to: L. Sorrentino (luigi.sorrentino@cnr.it).
Contract grant sponsor: MIUR (Italy) within the FIRB project MANTA; contract grant number: RBIP065YCL.

amount, nature, shape, particle size, aggregate size, and surface characteristics and the degree of dispersion in the polymer. In general, the mechanical properties of composites filled with nanometric particles are higher than those filled with micrometer-sized particles at the same filler content.[11–14] In addition, improvements in the physical properties, such as the surface smoothness and gas barrier properties, cannot be achieved with conventional micrometric particles. As a result, nanocomposites have attracted much interest because of their huge potential for providing novel performances. The tremendous interfacial area in a polymer nanocomposite helps to influence the composite's properties to a great extent, even at rather low filler loadings.[15] However, a homogeneous dispersion of nanoparticles is very difficult to achieve because nanoparticles with a high surface energy tend to agglomerate easily. To break up agglomerates, studies have been carried out on the *in situ* polymerization of monomers in the presence of nanoparticles[16–18] and other intercalation polymerization techniques.[19] These techniques are not very attractive for industry because of their low productivity, and the melt-blending technique is widely preferred.

Nanofillers can be used to control and enhance cell nucleation in foams, as widely investigated in the literature.[20,21] As clearly assessed, several difficulties are encountered in the production of nanocomposites based on engineering polymers through the melt-blending technique because of the very high processing temperatures needed. Conventional plateletlike nanofillers, such as montmorillonite, or fluorhectorite nanofillers based on organomodified ammonium salts cannot be used as cell nucleating agents in high-processing-temperature polymers because the degradation of the organic modifier occurs. As a result, the use of high-performance nanocomposite matrices has rarely been considered for the production of foams. For these applications, nonconventional organic modifiers or different types of nanofillers should be used.

To better understand the foaming process of polymers, the solid-state foaming technique, in which foaming is promoted by the dipping of samples in an oil bath at high temperatures after blowing agent solubilization, has been successfully employed.[3,5,10,22] This technique is very useful in the independent investigation of each foaming step: (1) solubilization of the blowing agent (usually a physical blowing agent) in the polymeric matrix, (2) generation of a thermodynamic instability in the solutions (by means of a sudden pressure drop or a temperature increase) to induce cell nucleation and growth, and (3) stabilization of the cellular structure through a viscosity increase.[22] Cell morphology and density of foams are significantly influenced by the blowing agent solubility, saturation pressure, foaming time, foaming temperature, and pressure drop rate and by the presence of nucleating agents, so the cellular microstructure can be tailored through the selection of appropriate foaming conditions and nucleating agents to produce foams with a wide range of densities and physical properties.[3–5]

The goal of this study was to investigate the effects of the nanofiller type (silica nanoparticles and expanded graphite) and their concentration on the foaming process of an amorphous engineering thermoplastic polymer [poly(ether sulfone)] (PES) and a semicrystalline one [poly(ethylene-2,6-naphthalate) (PEN)].

EXPERIMENTAL

PES (Ultrason E3010 from BASF, Ludwigshafen, Germany) and PEN (Teonex TN8065S from Teijin, Osaka, Japan) were used as high-performance polymers. Silica nanoparticles, Aerosil R380 (mean average primary particle size = 7 nm, specific surface area = 380 m^2/g), were furnished by Degussa-Evonik (Essen, Germany). Proprietary expanded graphite particles (platelet width < 65 μm, platelet thickness < 1 μm) were supplied by GrafTech International (TG-741, available exclusively from GrafTech International Holdings, Inc., Parma, OH). The blowing agent, carbon dioxide (purity = 99.9%, Società Ossigeno Napoli, Napoli, Italy), was used as received.

The nanoparticles were melt-mixed with polymers in a Haake Rheocord PTW25P twin-screw extruder (Karlsruhe, Germany) at 320°C for PES and 270°C for PEN at a screw speed of 40 rpm (5 min of residence time). Nanocomposite matrices with several filler contents (0.1, 0.5, 1.0, 2.0, and 2.5 vol %) were prepared. A hydraulic press (model P300P, from Collin Gmbh, Ebersperg, Germany) was used to prepare 500 μm thick samples through compression molding from nanocomposites. PEN-based samples were quenched from the melt state to obtain amorphous polymers to be used in the gas solubilization step. All analyzed samples were vacuum-dried at 120°C for 24 h before thermal analysis, gas absorption, and the foaming process.

Scanning electron microscopy (SEM) analysis on the nanofilled matrices and foams was performed on cryogenic fractured surfaces with a Leica S440 (Leica Microsystems, Wetzlar, Germany). All sample surfaces were gold-coated to render the specimen surfaces conductive.

Transmission electron microscopy (TEM) was carried out with a Philips EM 208 (Amsterdam, The Netherlands) at an acceleration voltage of 100 kV. We prepared samples for TEM analysis by cutting 70 nm thick films from PES matrices with an LKB ultramicrotome (LKB, Stockholm, Sweden). The dispersion of silica nanoparticles in the PES and PEN was examined by SEM and TEM. The expanded graphite particles exhibited electron densities very close to that of the polymer macromolecules, and therefore, the

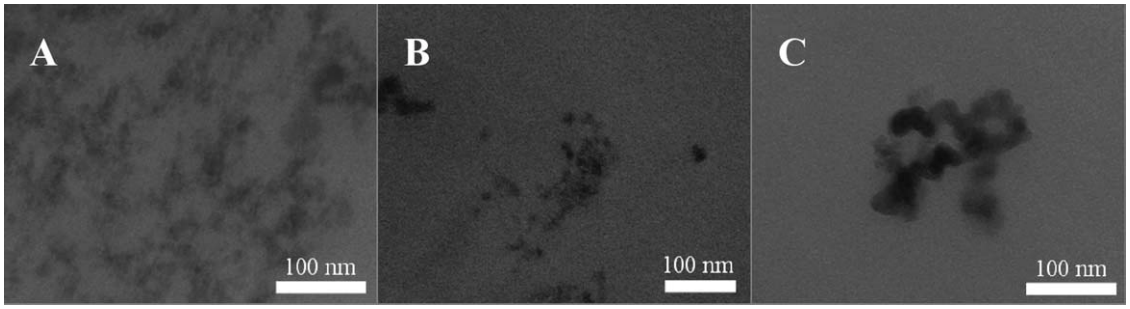

Figure 1 TEM image of PES + 0.5% SiO_2 sample with different morphologies of dispersed particles.

contrast of TEM images was inadequate to clearly evidence particles.

Graphite dispersion was investigated through an X-ray diffraction (XRD) analyzer at room temperature with a Philips X-ray generator and a Philips diffractometer (type PW1710). The X-ray beam was nickel-filtered Cu Kα radiation of wavelength 1.54 Å, operated with the voltage generator set to 40 kV and at a current of 20 mA. The diffraction intensity data were collected automatically at a scanning rate of 0.6°/min with 0.02°/s steps from 5 to 60°.

Thermal properties were evaluated with a differential scanning calorimeter (Q1000 DSC from TA Instruments, New Castle, DE). The glass-transition temperature (T_g), melting temperature (T_m), crystallization temperature (T_c), and crystallization enthalpy (ΔH_c) were determined by a heating scan from room temperature to 300°C at a heating rate of 10°C/min. The relative crystallinity (X_c) values were evaluated as the ratio ΔH_c to ΔH_m^o, where ΔH_m^o is the crystallization enthalpy of the perfect PEN crystal.[23]

Rheological tests were performed with an ARES rheometer from Rheometric Scientific (now TA Instruments), and master curves were calculated from rheological tests on PES samples at temperatures from 340 to 400°C in the frequency range between 0.1 and 10 Hz.

Gas absorption measurements were performed to evaluate the solubility of CO_2 in selected matrices. The solubilization of carbon dioxide was performed in a pressure vessel at 50°C and 80 bar, and the gas uptake was measured after 72 h by means of a high-precision balance.

The foaming procedure was as follows: the polymers were vacuum-dried at 120°C for 24 h and then saturated for 72 h in a pressure vessel with CO_2 at a pressure of 80 bar and a temperature of 50°C. Subsequently, the gas-saturated samples were removed from the vessel and dipped in an oil bath kept at the desired temperature for the time needed to reach the maximum expansion ratio (between 10 and 20 s, because longer times resulted in foam collapsing). The temperature range for the solid-state foaming process was from 200 to 260°C for both the amorphous and semicrystalline polymers.

Dynamic mechanical tests were carried out by means of a Triton DMA (Tritec 2000 from Triton, Grantham, United Kingdom) in tension configuration. The used heating rate was 4°C/min from 30 to 280°C, and the strain rate was 1 Hz. The samples were 30.0 mm in length, 6.0 mm in width, and 2.0 mm thick.

The densities of the foams were calculated as the ratio between the foam density (ρ_f; measured by the water-displacement method according to ASTM D 792) and the polymer bulk density. Because of the integral skin and closed-cell structure of all of the samples prepared, no water uptake was detected during the measurements.

The morphological parameters of the cellular structures were evaluated from SEM micrographs (SEM S440 from Leica Microsystems). In particular,

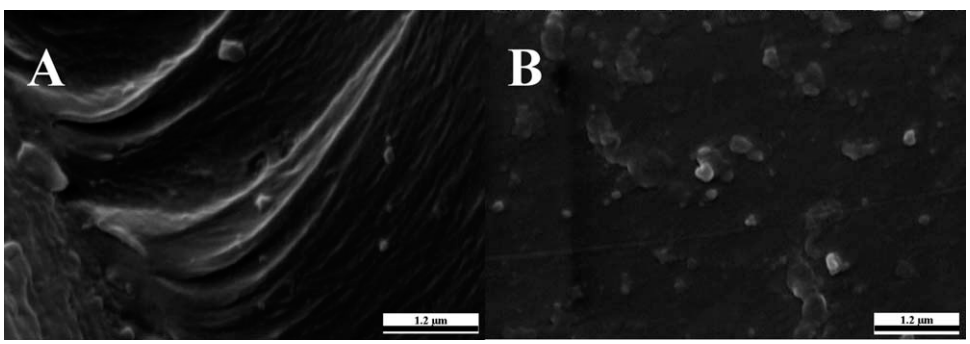

Figure 2 SEM images of cryogenically fractured (A) PES + 0.1% SiO_2 and (B) PES + 2.0% SiO_2 nanocomposites.

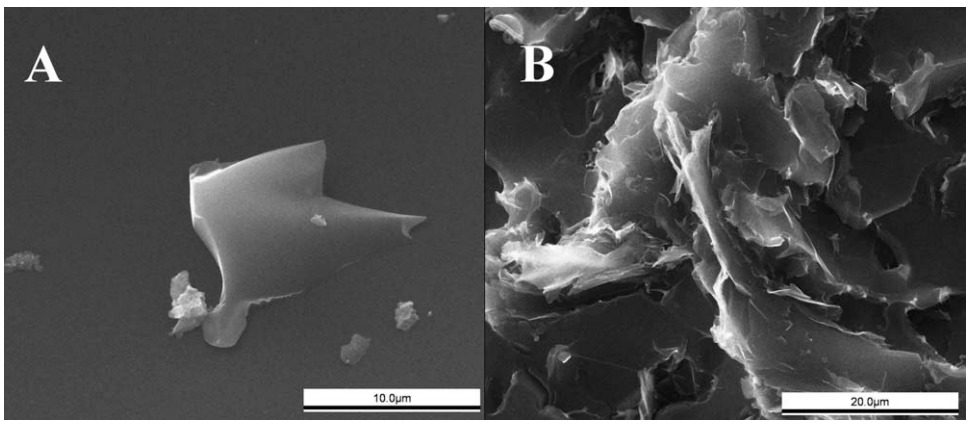

Figure 3 SEM images of cryogenically fractured (A) PES + 0.1% and (B) PES + 2.0% graphite nanocomposites.

the mean cell diameter was calculated over at least 50 measures, whereas N_0 was calculated with the following formula:[24]

$$N_0 = \left(\frac{n}{A}\right)^{\frac{3}{2}} \frac{1}{1+V_f} \quad (1)$$

with

$$V_f = 1 - \frac{\rho_f}{\rho_s} \quad (2)$$

where V_f is the void fraction of the foam, ρ_s is the bulk polymer density, n is the number of cells in the SEM micrograph, and A is the area of the micrograph (cm^2).

RESULTS AND DISCUSSION

SEM and TEM analyses

The matrices were analyzed by means of SEM, TEM, and XRD to verify the dispersion of the nanofillers. The TEM images in Figure 1 permitted us to distinguish different possible morphological arrangements of silica nanoparticles found in the prepared nanocomposites: (1) silica nanoparticles well dispersed in the PES matrix [Fig. 1(A)], (2) zones with agglomerates

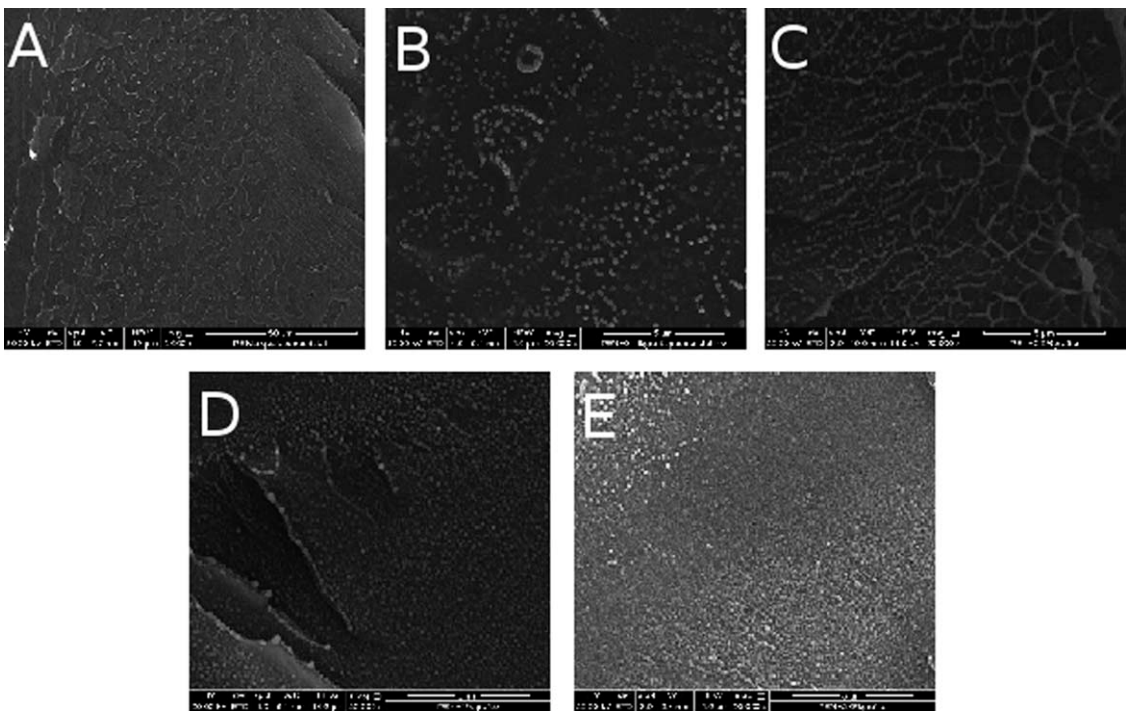

Figure 4 Fracture surfaces from SEM analysis of the PEN+graphite nanocomposites with (A) neat PEN, (B) 0.1% graphite, (C) 0.5% graphite, (D) 1.0% graphite, and (E) 2.5% graphite filler contents.

TABLE I
Number of Detected Objects Compared to the Theoretical Number of Platelets

Sample	Number of objects (number/cm^3)	Number of layers (layers/cm^3)
PEN + 0.1% graphite	2.8×10^{13}	1.5×10^{13}
PEN + 0.5% graphite	2.6×10^{14}	7.3×10^{13}
PEN + 1.0% graphite	3.1×10^{14}	1.5×10^{14}
PEN + 2.5% graphite	4.4×10^{14}	3.7×10^{14}

[Fig. 1(B)], and (3) wormlike silica agglomerates [Fig. 1(C)], such as those also reported in ref. 25. In the first two cases, both particles and clusters were smaller than 100 nm, whereas the wormlike agglomerates were characterized by a cross section of a few silica nanoparticles. They were less than 50 nm thick, even though the diameter of the spheroid, including the wormlike agglomerates, was longer than 100 nm.

SEM examinations of the cryogenically fractured surfaces of silica nanocomposites revealed the presence of clusters whose number and size increased with the filler content (Fig. 2), but the dimensions of the agglomerates never exceeded 600 nm.

SEM images of the cryogenically fractured surfaces of PES samples containing expanded graphite showed the presence of platelets of different dimensions [Fig. 3(A)]. Graphite platelets, about 30 nm thick and partially embedded in the PES matrix, are shown in Figure 3(B). PES/graphite samples also exhibited some clusters of nanoparticles of different platelet sizes with increasing filler content and showed difficulty in achieving a high dispersion degree with higher filler loadings.

SEM and TEM investigations indicated a good dispersion of nanoparticles (for both silica and graphite) at the nanoscale level, as well as the occasional occurrence of agglomerates. The size of nanosilica agglomerates ranged from 100 to 500 nm, and the width of some graphite nanoparticles was higher than 10 μm. The dispersion of silica nanoparticles in the PEN-based matrices presented features similar to those of PES; as a consequence, their SEM and TEM images are not reported.

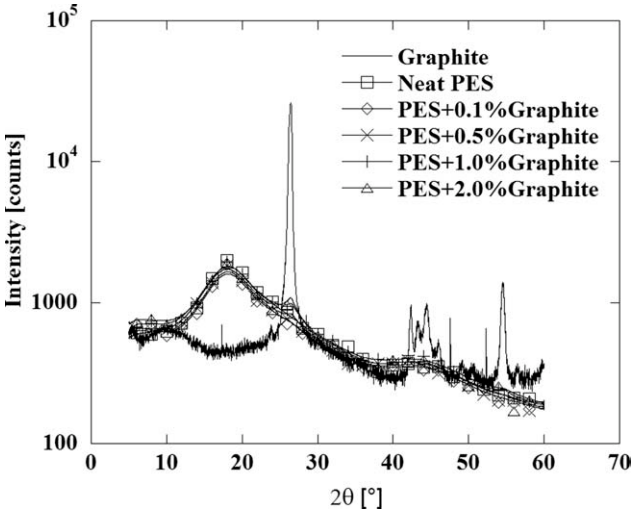

Figure 6 XRD patterns of the PES/graphite nanocomposites and graphite powder

SEM investigations of the PEN/graphite nanocomposites showed good dispersion of graphite platelets, and unlike in the PES/graphite samples, single platelets were not evident. Graphite induced in the PEN matrix the formation of spherical objects (Fig. 4) of nanometric dimensions (average dimension = 200 nm).

The theoretical number per unit volume of graphite layers was calculated with geometrical parameters from an expanded graphite technical datasheet. The platelets were considered as discoids, with a diameter equal to 500 nm, an average distance between layers of 30 nm, and a thickness of a single platelet equal to 34 nm. The number of layers per unit

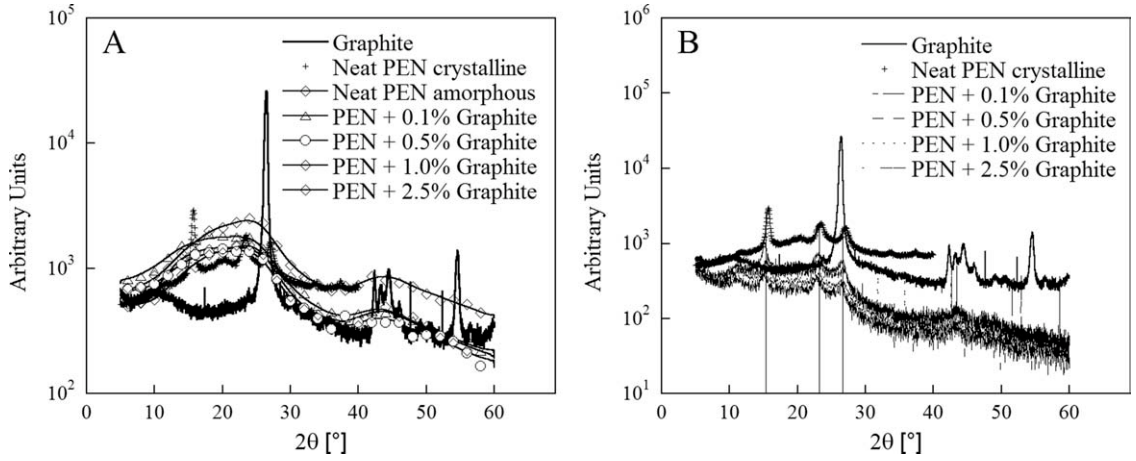

Figure 5 XRD patterns of the PEN nanocomposites, neat PEN in the amorphous and semicrystalline states, and graphite powder: (A) untreated and (B) foamed.

TABLE II
T_g Values of the Prepared Samples

Sample	T_g (°C)
Neat PES	229.57
PES + 0.1% SiO_2	229.94
PES + 0.5% SiO_2	230.33
PES + 1.0% SiO_2	230.06
PES + 2.0% SiO_2	230.37
PES + 0.1% graphite	230.10
PES + 0.5% graphite	230.47
PES + 1.0% graphite	229.89
PES + 2.5% graphite	230.27

volume was calculated and compared to the number of objects detected in the SEM images (Table I), and good agreement was evidenced.

XRD analysis

XRD analysis was conducted on the PES and PEN nanocomposites to get over the difficulty of investigating the expanded graphite nanoplatelet dispersion in the nanocomposite matrices with the TEM technique. The PEN nanocomposites were analyzed after a quenching process from the melt state to avoid superposition of the crystalline phase peaks with the graphite main peak. In Figure 5, wide-angle XRD patterns of the PEN nanocomposites (including neat PEN in the amorphous and crystalline states) and of graphite powder are compared before [Fig. 5(A)] and after foaming [Fig. 5(B)]. It was evident that before foaming, all nanocomposites did not show peaks corresponding to crystal reflections, whereas after foaming, all samples showed the characteristic peaks of the crystalline phase. The PES samples showed similar XRD behavior (Fig. 6), with only a hint of a graphite peak at higher loadings, because of the presence of incompletely exfoliated graphite platelets.

The absence of the peak at 26.7° in all of the XRD patterns of PEN nanocomposites, coupled with the absence of visible platelets in high-resolution SEM images and with the proportionality of spherules to theoretical values of exfoliated platelets, was indirect evidence of the good dispersion of expanded graphite nanoparticles at all filler concentrations.

TABLE IV
Blowing Agent Uptake of the Nanocomposite Matrices

	CO_2 uptake (wt %)			
	Graphite		SiO_2	
Nanofiller content (%)	PEN	PES	PEN	PES
Neat	5.2	6.5	5.2	6.5
0.1	4.8	6.2	5.2	6.5
0.5	4.1	6.2	5.2	6.7
1.0	4.5	5.8	4.3	6.4
2.0			4.4	6.7
2.5	3.5	4.6		

DSC measurements

Thermal properties of the polymeric matrices were evaluated because of their role in the foaming process, in particular for PEN-based samples. In fact, fast crystallization kinetics could have helped to stabilize the cellular structure but also hindered the matrix expansion. A heating scan was performed on the PES nanocomposites to evaluate T_g. As shown in Table II, the T_g values of the PES nanocomposites were not significantly affected by silica or graphite nanoparticles, with its variations within ±0.5°C with respect to T_g of the neat polymer.

The crystallization kinetics of the PEN nanocomposites were qualitatively estimated by means of a heating–cooling DSC double-scan procedure. The first scan from quenched polymers was used to evaluate the degree of crystallinity in samples used for the foaming process (Table III). Small values of ΔH_c were evidenced for all of the nanocomposites. The

TABLE III
Thermal Properties from the Heating Scans (from the Quenched State) and Cooling Scans (from the Melt State) after Foaming (T_{foam} = 240°C) of the PEN Nanocomposites

	Heating from the quenched state	Cooling from the melt state		After foaming (T_{foam} = 240°C)
	X_c (%)	X_c (%)	T_c (°C)	X_c (%)
Neat PEN	5.0	2.8	187.0	7.4
PEN + 0.1% SiO_2	3.1	3.5	181.0	
PEN + 0.5% SiO_2	3.3	2.6	187.0	
PEN + 1.0% SiO_2	3.2	2.6	184.0	
PEN + 0.1% graphite	4.3	19.9	205.9	18.2
PEN + 0.5% graphite	5.0	18.7	205.0	14.9
PEN + 1.0% graphite	3.4	17.7	201.6	15.9
PEN + 2.5% graphite	3.1	16.7	205.3	14.8

T_{foam}, foaming temperature.

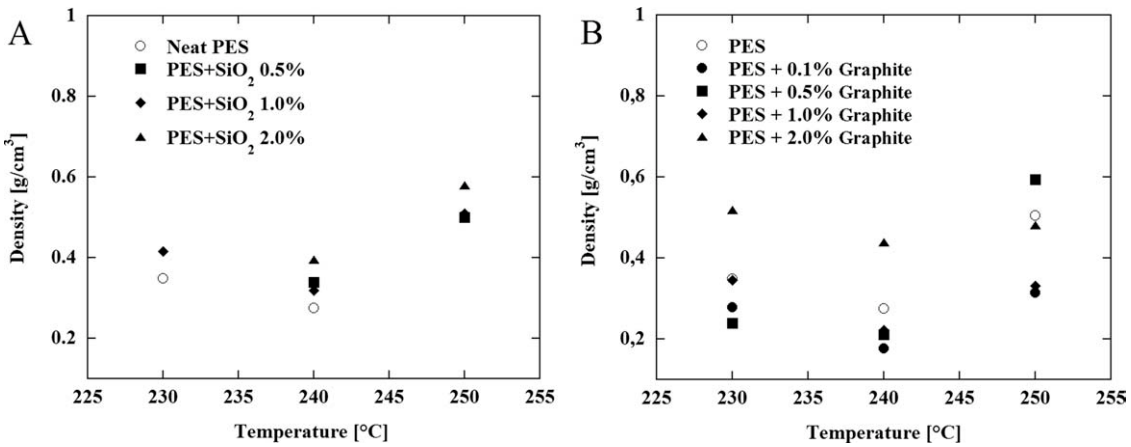

Figure 7 Densities of the PES nanocomposite foams as a function of the foaming temperature for (A) SiO_2 and (B) graphite nanoparticles.

small amount of crystallinity did not hinder the foaming of the matrices.

A cooling scan for each composition was performed to evaluate the crystallinity and to qualitatively compare the crystallization rate during cooling from the melt state. The graphite-based nanocomposites showed the highest degree of crystallinity and exhibited crystallization peaks from the melt state at temperatures higher than 200°C, whereas the nanosilica-based nanocomposites presented reduced crystallinity with a crystallization peak temperature around 185°C (Table III). Graphite was very effective as a crystallization kinetics enhancer, and this thermal behavior had consequences on the foaming process of the PEN-based samples.

Absorption properties

The amount of foaming agent dissolved in the matrices was measured at the end of the blowing agent solubilization, and the CO_2 uptake in all of the matrices is reported in Table IV. The PEN samples presented a lower CO_2 uptake with respect to the PES samples, partially because of the small amount of crystalline phase (see Table III). The presence of silica nanoparticles did not affect the gas sorption in the PES samples, whereas it reduced the sorption of CO_2 in the PEN nanocomposites at higher nanofiller loadings. On the contrary, graphite platelets always reduced the gas uptake with increasing filler content, in particular for PEN nanocomposites.

As reported in a previous work,[26] silica nanoparticles induced a weak reduction of carbon dioxide diffusivity in the PES + 0.1% SiO_2 system, whereas graphite platelets acted as barrier to gas diffusion, inducing a 40% reduction of the diffusivity coefficient at the same filler content. The contribution of diffusivity to the foaming properties of the nanocomposite samples is discussed in the following text.

Foams morphology: PES nanocomposites

The ρ_f's, cell densities, and morphologies of the samples prepared through the solid-state process were evaluated and related to the matrix composition and processing conditions. The densities of the PES

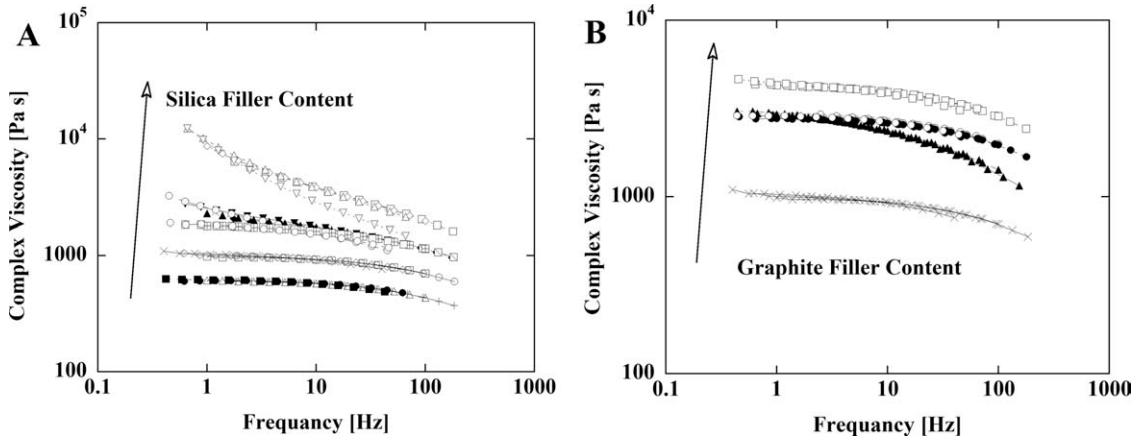

Figure 8 Master curves of complex viscosity for PES-based nanocomposites: (A) silica and (B) graphite based.

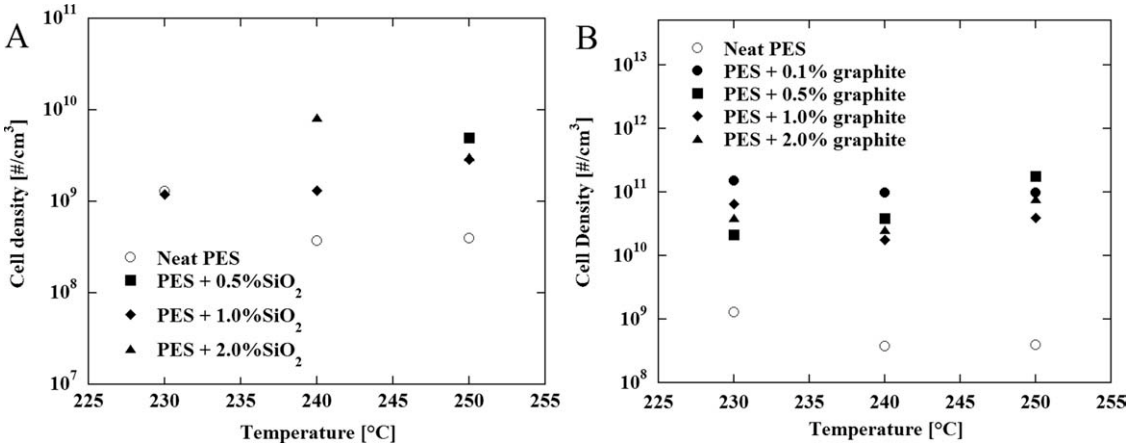

Figure 9 Cell densities of the PES nanocomposite foams as a function of the foaming temperature for (A) SiO_2 and (B) graphite nanoparticles.

nanocomposites (Fig. 7), plotted as function of the foaming temperature, showed that the density of the neat PES foams was not lower than 0.27 g/cm^3. The addition of nanosilica slightly increased the density with respect to the neat polymer. This was addressed to the increase of the viscosity with filler content (Fig. 8). The graphite nanocomposites exhibited a different behavior, giving a density reduction of around 30% for samples filled with 0.1 to 1.0% nanofiller. At the highest graphite content, the high viscosity induced low expansion ratios. It is worth noting that in all cases, a minimum of the density curve was present.

The effect of the two nanofillers was particularly evident on cell nucleation during foaming (Fig. 9). Both nanosilica and graphite nanoparticles enhanced the nucleation rate, acting as heterogeneous sites, but graphite was much more effective at all filler loadings. This behavior was due to (1) the higher number of dispersed graphite platelets, which resulted in a lower number of particle aggregates with respect to silica nanoparticles, (2) the different interfacial energy of particles with the polymeric matrix, and (3) the reduction of the gas diffusivity coefficient,[13,26] which hindered CO_2 molecule migration through the polymeric matrix and produced smaller cells. The best results were obtained for 0.1% filled samples (Fig. 10), which exhibited a two order of magnitude increase of cell number, from 10^9 to 10^{11} cells per cm^3. In Figure 11, a comparison between the SEM micrographs of two nanocomposite samples are presented to show the microcellular, closed-cell morphology developed during the foaming process.

Foam morphology: PEN nanocomposites

The densities of the PEN-based foams were lower than those exhibited by the PES nanocomposites (Fig. 12). The SiO_2-filled matrices exhibited densities that were slightly lower than those of neat PEN at every foaming temperature, except at 240°C for the

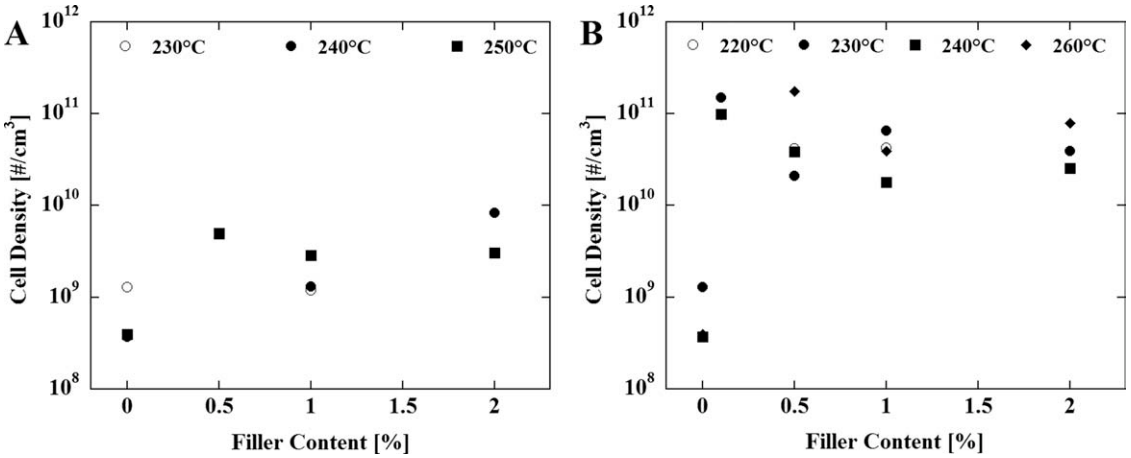

Figure 10 Nucleating efficiency of (A) silica and (B) graphite nanoparticles as function of the filler content.

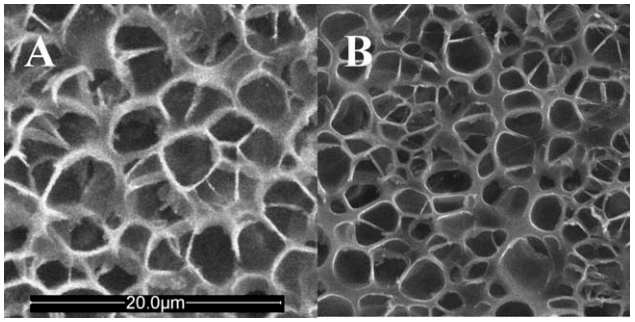

Figure 11 Comparison of the SEM micrographs of foams from (A) PES + 2.0% SiO_2 and (B) PES + 0.1% graphite nanocomposites.

2.0% filled sample. The graphite-filled matrices showed a different behavior: ρ_f values were higher than those exhibited by the neat polymer samples, with the exception of the 0.1% filled samples and for all nanocomposite samples foamed at 200°C. Furthermore, the density values of the nanocomposite foams increased with the temperature. This behavior was related to the effect of graphite nanoplatelets on the PEN crystallization kinetics, which were stronger with respect to the silica nanoparticles, as evidenced in Table III. At all concentrations, graphite platelets increased the crystallization kinetics (higher T_c from the melt state during cooling) of the polymeric matrix, and the crystallinity of the nanocomposite samples was higher than that of the neat PEN samples (in Table III, X_c after foaming at 240°C is shown). As a result, fast crystalline phase development during the foaming process hindered the density reduction. This approach was also confirmed by data from dynamic mechanical analysis (Fig. 13) of quenched samples, where a fast crystallization during heating was clearly evident for all graphite concentrations.

The use of silica nanoparticles reduced cell nucleation with respect to those nucleated in the neat polymer [Fig. 14(A)] at each foaming temperature, but

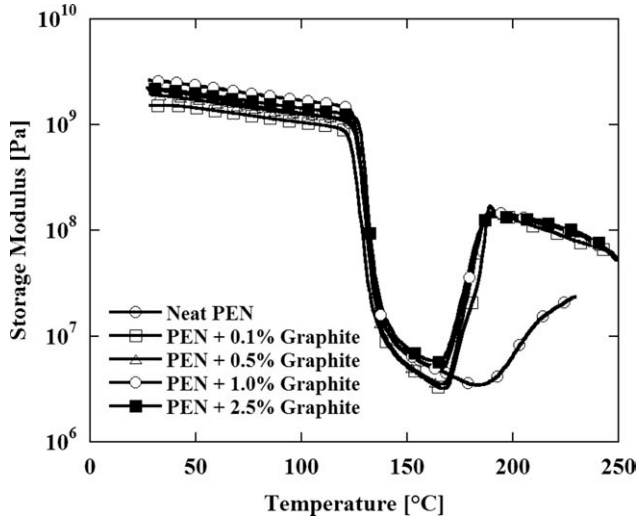

Figure 13 Comparison of the storage modulus values of the neat PEN and PEN nanocomposites.

0.1% filled samples showed the highest cell densities among the silica nanocomposites [Fig. 15(A)]. The graphite nanocomposites showed better or comparable results in some conditions with respect to the neat polymer samples at each foaming temperature [Fig. 14(B)], and in quite all processing conditions, the best results were shown at 0.1% filler content [Fig. 15(B)].

In Figure 16, a comparison between the cellular morphologies of the PEN + 0.1 SiO_2 and PEN + 0.1% graphite samples is shown. Large cells were produced in the silica-based nanocomposite foams, whereas a microcellular morphology was obtained from the graphite-filled matrix. This behavior could be explained by the cell coalescence in the nanosilica systems due to the weak contribution of nanoparticles to the cell stabilization. On the contrary, the fast formation of the crystalline phase promoted by the graphite platelets prevented the coalescence of the cells and allowed the stabilization of the cellular morphology.

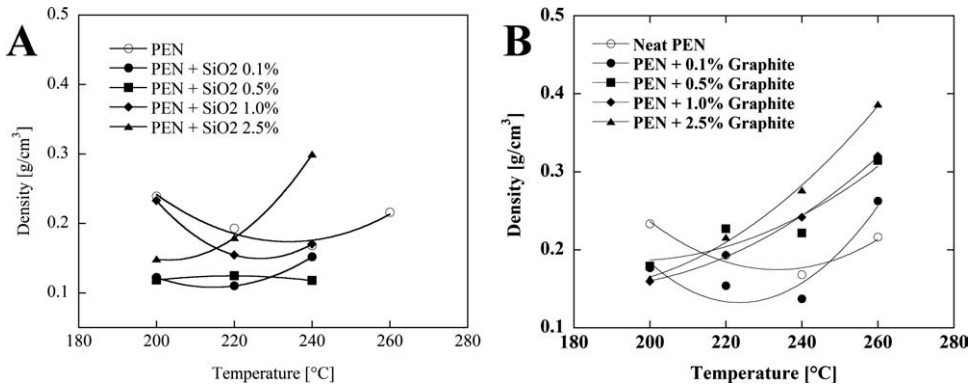

Figure 12 Densities of PEN nanocomposite foams as a function of the foaming temperature for (A) SiO_2 and (B) graphite nanoparticles.

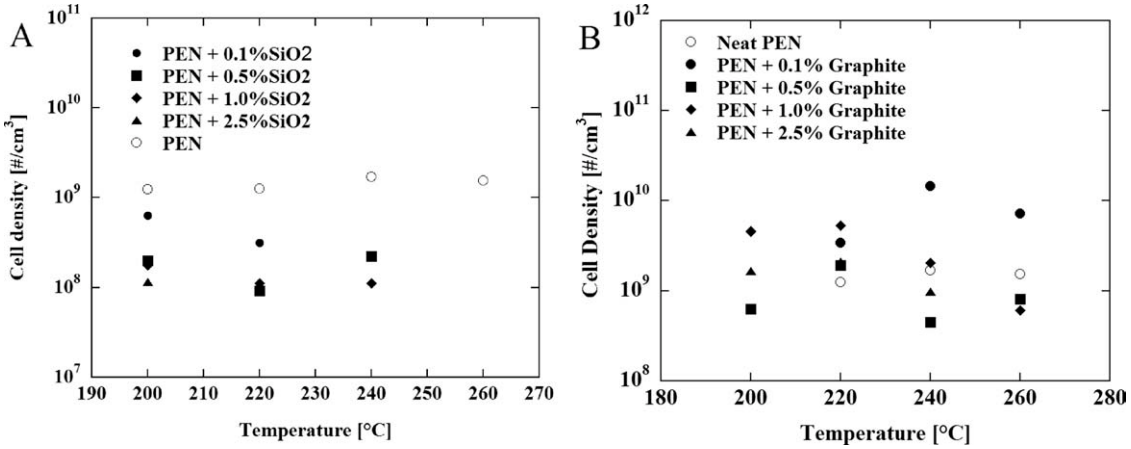

Figure 14 Cell densities of the PEN nanocomposite foams as a function of the foaming temperature for (A) SiO_2 and (B) graphite nanoparticles.

A direct proportionality between the filler content and the number of nucleated cells was not present in any of the nanocomposite systems. Graphite nanoparticles exhibited at the lowest filler content (0.1%), in all used processing conditions, an amount of nucleated cells one order of magnitude higher than that showed by unfilled samples; a further increase of the nanoparticle content in the matrix did not result in more sites useful for nucleating bubbles. When silica nanoparticles were used, the growing amount of aggregates of different dimensions and distributions in the polymeric matrices with increasing filler content was responsible for the leveling of the number of nucleated cells.

As a final consideration, the comparison of the nucleating efficiency of silica and graphite nanoparticles showed that graphite nanoparticles allowed a gain of one order of magnitude with respect to silica nanoparticles in both the PES- and PEN-based nanocomposites and that the lowest filler content (0.1%) was able to maximize the nucleated cells.

CONCLUSIONS

Nanocomposites based on PES and PEN matrices were successfully prepared with silica and graphite nanoparticles and were used as matrices for the production of foams. Both type of nanofillers were dispersed at the nanoscale and generally acted as heterogeneous cell nucleating agents during the foaming process. The PES nanocomposites exhibited higher cell densities with respect to the PEN ones, but ρ_f was significantly higher. The graphite nanoparticles exhibited the strongest nucleating efficiency, inducing an increase in cell densities one order of magnitude higher than that measured in the silica nanocomposites (either based on PES or PEN matrices) with the same nanofiller content.

The foaming properties of the PEN nanocomposites were affected by the development of the crystalline phase. The presence of silica nanoparticles slightly influenced the crystallization kinetics, giving X_c values comparable to those exhibited by the neat polymer, and a reduction of ρ_f at each foaming

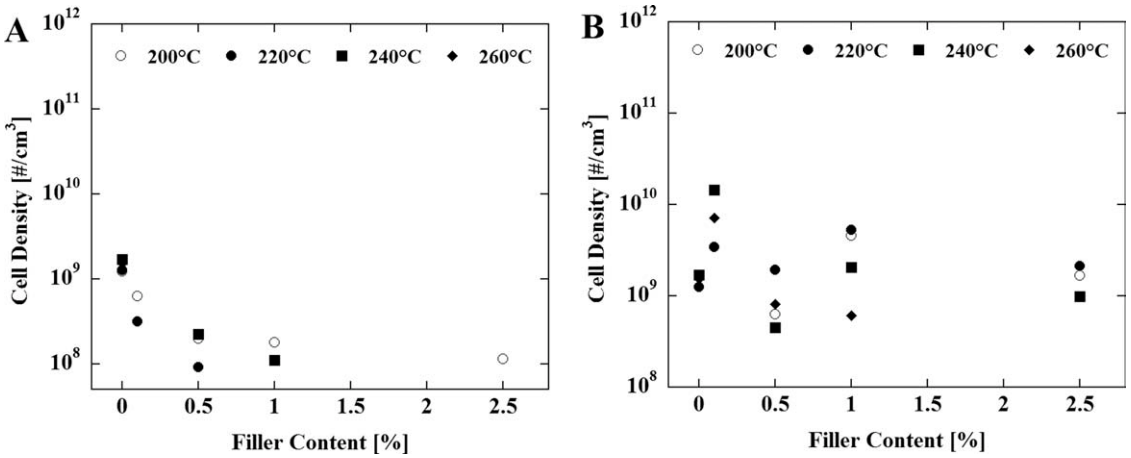

Figure 15 Cell density versus filler content for the (A) SiO_2 and (B) graphite nanocomposites.

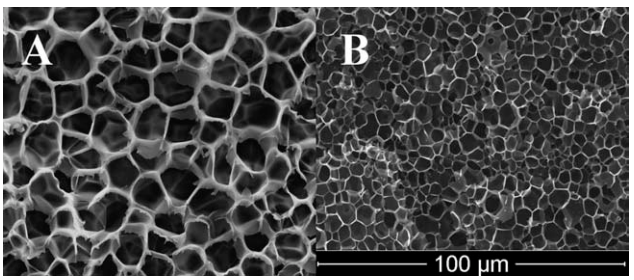

Figure 16 Comparison of SEM micrographs of foams from the (A) PEN + 0.1% SiO_2 and (B) PEN + 0.1% graphite nanocomposites.

temperature was obtained. Conversely, graphite induced the formation of crystalline phase, even during nanocomposite quenching. The strong increase of the crystallization rate blocked cell growth, and higher ρ_f values with respect to neat polymer samples were induced at foaming temperatures higher than 200°C.

The authors thank Vincenzo Scognamiglio for contributing to all of the experimental activities.

References

1. Gibson, L. J.; Ashby, M. F. Cellular Solids: Structure and Properties, 2nd ed.; Cambridge University Press: Cambridge, England, 1997.
2. Mascia, L.; Del Re, G.; Ponti, P. P.; Bologna, S.; Di Giacomo, G.; Haworth, B. Adv Polym Tech 2006, 25, 225.
3. Hongliu, S.; Mark, J. E. J Appl Polym Sci 2002, 86, 1692.
4. Hongliu, S.; Sur, G. S.; Mark, J. E. Eur Polym J 2002, 38, 2373.
5. Sorrentino, L.; Di Maio, E.; Iannace, S. J Appl Polym Sci 2010, 116, 27.
6. Colton, J. S.; Suh, N. P. Mater Manuf Process 1986, 1, 341.
7. Jonathan, S.; Colton, J. S.; Suh, N. P. Polym Eng Sci 1987, 27, 500.
8. Hiroaki, Y.; Shigeru, Y. [to UBE Industries (Japan)]. U.S. Pat. 6,576,683 (2003).
9. Airex C71 Datasheet; Alcan Composites: Sins, Switzerland, 2005.
10. Sorrentino, L.; Aurilia, M.; Iannace, S. Adv Polym Tech, to appear.
11. Sumita, M.; Tsukurmo, T.; Miyasaka, K.; Ishikawa, K. J Macromol Sci Phys 1983, 22, 601.
12. Sumita, M.; Tsukurmo, T.; Miyasaka, K.; Ishikawa, K. J Mater Sci 1983, 18, 1758.
13. Aurilia, M.; Sorrentino, L.; Sanguigno, L.; Iannace, S. Adv Polym Tech 2010, 29, 146.
14. Sorrentino, L.; Berardini, F.; Capozzoli, M. R.; Amitrano, S.; Iannace, S. J Appl Polym Sci 2009, 113, 3360.
15. Dagani, R. Chem Eng News 1999, 77, 25.
16. Akelah, A. J Mater Sci 1996, 13, 3589.
17. Lee, D. C. J Appl Polym Sci 1996, 7, 1117.
18. Gray, H. Adv Mater 1997, 9, 731.
19. Rong, M.; Zhang, M.; Zhang, Y. J Mater Sci Lett 2000, 19, 1159.
20. Ramesh, N. S.; Lee, S. T. Cell Polym 2005, 24, 269.
21. Marrazzo, C.; Di Maio, E.; Iannace, S. Polym Eng Sci 2008, 48, 336.
22. Klempner, D.; Sendjarevic, V. Polymeric Foams and Foam Technology, 2nd ed.; Hanser: New York, 2000.
23. Buchner, S.; Wiswe, D.; Zachmann, H. G. Polymer 1989, 30, 480.
24. Gosselin, R.; Rodrigue, D. Polym Test 2005, 24, 1027.
25. Nanocomposite Science and Technology; Ajayan, P. M., Schadler, L. S., Braun, P. V., Eds.; Wiley-VCH: Weinheim, 2003.
26. Pastore Carbone, M. G.; Catapano, A.; Fariello, M. L.; Aurilia, M.; Sorrentino, L.; Di Maio, E.; Iannace, S.; Mensitieri G. Presented at VII INSTM National Conference on Material Science and Technology, Tirrenia (PI), Italy, December 2009.